

# Nonlinear Lindblad Master Equation and Postselected Skin Effect

Yu-Guo Liu<sup>1</sup> and Shu Chen<sup>1,2,\*</sup>

<sup>1</sup>Beijing National Laboratory for Condensed Matter Physics,  
Institute of Physics, Chinese Academy of Sciences, Beijing 100190, China

<sup>2</sup>School of Physical Sciences, University of Chinese Academy of Sciences, Beijing 100049, China  
(Dated: May 21, 2024)

We introduce a non-linear Lindblad master equation to describe the postselection dynamics of open quantum systems described by the Lindblad master equation, which continuously interpolates between the Lindblad master equation and the dynamical equation governed by an effective non-Hermitian Hamiltonian. Within the framework of the non-linear Lindblad master equation, we study a prototypical model and demonstrate the existence of the postselected skin effect with the distribution of a steady state characterized by the accumulation of particles on one side, as long as some quantum jumping terms are discarded by postselection processes. Moreover, we show that the trajectory-averaged entanglement entropy can reflect the different influences from the environment and postselection, and unveil it exhibiting a special distribution with algebraic growth in the short chain and saturation in the long chain induced by the postselected skin effect.

**Introduction.**— The Lindblad master equation (LME) governed by Liouvillians and the dynamical equation governed by effective non-Hermitian Hamiltonians are two kinds of linear differential equations that are widely utilized in the study of non-equilibrium quantum physics. While the former describes the dynamics of open quantum systems under the Born-Markov approximation [1–4], the latter can be viewed as a short-time approximation. Formally, the Liouvillian can be separated into two parts: the effective non-Hermitian Hamiltonian and quantum jumps. In order to describe quantum dynamics properly, usually jump terms can not be ignored [5]. The interplay of the non-Hermitian Hamiltonian and quantum jumps provides a way of understanding the LME as an average of quantum trajectories consisting of the evolution of non-Hermitian Hamiltonian (ENHH) and random quantum jumps. This interpretation leads to the quantum trajectory method or Monte Carlo wave-function method, which was originally proposed as a numerical method for simulating dissipative dynamics in the early 1990s [6–11]. Interestingly, the jumps and trajectories are caught in the experiments in the following decades [12–17]. In recent years, the dynamics of trajectory-averaged entanglement entropy have been paid great attention to. The entanglement growth and phase transition are studied in random quantum circuits [18–23], under continuous monitoring [24–28], and systems with non-Hermitian skin effect [29–35], etc.

If postselecting the quantum trajectories with no jumps, the LME transfers to ENHH, which is often regarded as a method to obtain the dynamics governed by the Non-Hermitian Hamiltonian. However, finding a pure non-Hermitian trajectory without jumps is difficult due to the probability tending to zero with increasing observation time and jump operators. Since the difficulty of excluding all jumps, we aim to study the non-unitary dynamics by partly getting rid of jumps. In Ref. [36], a hybrid-Liouvillian formalism has been proposed to explore the relation between non-Hermitian Hamiltonian and Liouvillian exceptional points. However, the transition of dynamics between LME and ENHH has not been explored. In this work, we introduce a nonlinear Lindblad master equa-

tion to describe the dynamics of an open system lacking an arbitrary proportion of quantum jumps. This equation continuously interpolates between LME and ENHH and can be realized by postselecting the quantum trajectories. We analyze its properties and classify it into trivial and nontrivial classes according to whether it can be reduced to a linear LME. In the nontrivial class, a prototypical model is given to showcase the postselected skin effect, where particles of non-equilibrium steady state will accumulate on one side as long as an arbitrarily small proportion of quantum jumps is discarded by postselection. Here the postselected skin effect refers to the steady state with skin effect induced by postselection processes, which is different from either the non-Hermitian skin effect [37–39] or previously studied dynamical skin effect [40–42] and Liouvillian skin effect [43, 44] in open quantum systems. Although increasing either the environmental coupling or postselection efficiency can enhance the postselected skin effect, they lead to the trajectory-averaged entanglement entropy (TAEE) exhibiting different features.

**Nonlinear Lindblad master equation.**— Considering a system with Hamiltonian  $H$  coupling to the environment by  $M$  jump operators  $L_\mu$  with strength  $\gamma_\mu$ , its density matrix  $\rho$  is governed by LME:

$$\frac{d\rho}{dt} = \mathcal{L}(\rho) := -i[H, \rho] + \sum_{\mu=1}^M \gamma_\mu \left( L_\mu \rho L_\mu^\dagger - \frac{1}{2} \{L_\mu^\dagger L_\mu, \rho\} \right), \quad (1)$$

where  $\mathcal{L}$  is the Liouvillian superoperator and Planck constant  $\hbar$  is set to unity throughout this paper. We monitor every jump by a  $\eta_\mu$ -efficiency detector,  $\eta_\mu \in [0, 1]$ , as shown in Fig. 1 (a). The core concern of the present work is how  $\rho$  evolves after discarding the data along with detectors clicking.

The equation of motion is derived in the spirit of the quantum trajectory method [45]. At time  $t$ , the system is assumed in a pure state  $|\phi(t)\rangle$ . Postselecting the data after  $\delta t$ , the  $L_\mu$  will make the system jump to the state  $\mathcal{N}L_\mu|\phi(t)\rangle$  with the probability of  $(1 - \eta_\mu)\delta p_\mu$  or evolve to the state  $\mathcal{N}exp(-\frac{1}{2}\gamma_\mu L_\mu^\dagger L_\mu \delta t)|\phi(t)\rangle$ , where  $\mathcal{N}$  denotes normalization

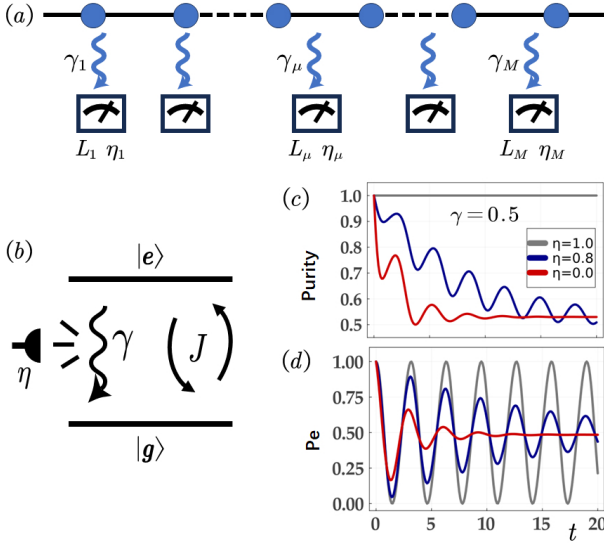


FIG. 1. (a) Illustration of the postselection experiment. The system is coupled to the environment by jump operators  $L_\mu$  with coupling strength  $\gamma_\mu$ . Every jump is monitored by a detector with efficiency  $\eta_\mu$ . Only the experimental data with no quantum jumps detected is preserved. (b) Postselection on a two-level atom with spontaneous emission. Emission photons are detected with efficiency  $\eta$ . Initialize the atom at  $|e\rangle$ . Observe the population of two levels. Discard the observed data when a photon is detected at the same time. After the postselection, the purity of the atomic density matrix  $\text{Tr}(\rho^2)$  and the probability of  $|e\rangle$  are shown in (c) and (d). With increasing  $\eta$  from 0 (red line) to 0.8 (blue line) and then to 1 (grey line), the purity increases and Rabi oscillation time becomes longer. In (c) and (d),  $J = 1$  and  $\gamma = 0.5$

and  $\delta p_\mu = \gamma_\mu \delta t \langle \phi(t) | L_\mu^\dagger L_\mu | \phi(t) \rangle$ . Then the state at time  $t + \delta t$  is

$$|\phi(t + \delta t)\rangle = e^{-iH\delta t} \mathcal{N} \prod_{\mu=1}^M \left\{ \begin{array}{l} (1 - \eta_\mu) \delta p_\mu : L_\mu \\ 1 - (1 - \eta_\mu) \delta p_\mu : e^{-\frac{1}{2} \gamma_\mu L_\mu^\dagger L_\mu \delta t} \end{array} \right\} |\phi(t)\rangle. \quad (2)$$

The error from the non-commutativity among different jump operators and Hamiltonian is ignored with  $\delta t \rightarrow 0$ . By using

$$\frac{d}{dt} \rho = \lim_{\delta t \rightarrow 0} \frac{1}{\delta t} (|\phi(t + \delta t)\rangle \langle \phi(t + \delta t)| - |\phi(t)\rangle \langle \phi(t)|), \quad (3)$$

we get the nonlinear Lindblad master equation:

$$\begin{aligned} \frac{d}{dt} \rho &= \mathcal{L}_\eta(\rho) := -i[H, \rho] + \\ &\sum_{\mu=1}^M \gamma_\mu \left( -\frac{1}{2} \langle L_\mu^\dagger L_\mu, \rho \rangle + (1 - \eta_\mu) L_\mu \rho L_\mu^\dagger + \eta_\mu \langle L_\mu^\dagger L_\mu, \rho \rangle \right), \end{aligned} \quad (4)$$

where the nonlinear term  $\langle L_\mu^\dagger L_\mu, \rho \rangle = \text{Tr}(L_\mu^\dagger L_\mu \rho)$  comes from the normalization process. From the perspective of postselection, it is natural to rewrite Eq. (4) as a combination of effective non-Hermitian Hamiltonian  $H_{eff}$  and quantum jumps  $\mathcal{L}_{QJ}$ :

$$\frac{d}{dt} \rho = -iH_{eff}(\gamma)\rho + i\rho H_{eff}^\dagger(\gamma) + \mathcal{L}_{QJ}(\rho) + \mathcal{L}_N(\rho), \quad (5)$$

where

$$H_{eff}(\gamma) = H - \frac{i}{2} \sum_{\mu} \gamma_\mu L_\mu^\dagger L_\mu, \quad (6a)$$

$$\mathcal{L}_{QJ}(\rho) = \sum_{\mu} (1 - \eta_\mu) \gamma_\mu L_\mu \rho L_\mu^\dagger, \quad (6b)$$

$$\mathcal{L}_N(\rho) = \sum_{\mu} \eta_\mu \gamma_\mu \langle L_\mu^\dagger L_\mu, \rho \rangle, \quad (6c)$$

where  $\mathcal{L}_N$  is the normalization term. Alternatively, Eq. (4) can also be represented as a combination of effective non-Hermitian Hamiltonian and pure measurements  $\mathcal{L}_M$ :

$$\frac{d}{dt} \rho = -iH_{eff}(\eta\gamma)\rho + i\rho H_{eff}^\dagger(\eta\gamma) + \mathcal{L}_M(\rho) + \mathcal{L}_N(\rho), \quad (7)$$

where

$$H_{eff}(\eta\gamma) = H - \frac{i}{2} \sum_{\mu} \eta_\mu \gamma_\mu L_\mu^\dagger L_\mu, \quad (8a)$$

$$\mathcal{L}_M(\rho) = \sum_{\mu} (1 - \eta_\mu) \gamma_\mu \left( L_\mu \rho L_\mu^\dagger - \frac{1}{2} \langle L_\mu^\dagger L_\mu, \rho \rangle \right). \quad (8b)$$

The simplest model for Eq. (4) is a two-level atom with monitoring its spontaneous emission, as shown in Fig. 1 (b), where  $J$  is the coupling strength and  $\gamma$  is the spontaneous emission rate of the excited state  $|e\rangle$ . The detector of emission photons has a finite efficiency  $\eta$ . In the experiment, the observed data of atomic population is discarded when emission photons are detected simultaneously. With the remaining data, the evolution of atomic system is rebuilt by

$$\frac{d}{dt} \rho = -i[H, \rho] + \gamma \left( -\frac{1}{2} \langle L^\dagger L, \rho \rangle + (1 - \eta) L \rho L^\dagger + \eta \langle L^\dagger L, \rho \rangle \right), \quad (9)$$

where  $H = J(|e\rangle\langle g| + h.c.)$  and  $L = |g\rangle\langle e|$ . A vectorization treatment of Eq. (9) is given in the Supplemental Material [45]. With increasing  $\eta$ , the quantum jumps after postselection decrease, the purity of atomic state becomes larger in Fig. 1 (c) and the coherence time characterized by Rabi oscillation becomes longer in Fig. 1 (d).

**Properties and classification.**— The NLME given by Eq. (4) provides a convenient method to study the postselection dynamics. Before going to the study of concrete systems, we discuss some specific features of the NLME. Firstly, we show some properties of NLME.

Property I:  $\mathcal{L}_\eta(\rho)^\dagger = \mathcal{L}_\eta(\rho^\dagger)$ . If the initial density matrix is Hermitian, i.e.  $\rho_0^\dagger = \rho_0$ , the NLME is Hermiticity-preserving, i.e.  $\rho(t)^\dagger = \rho(t)$ , where  $\rho(t) = e^{\mathcal{L}_\eta t} \rho_0$ .

Property II:  $\frac{d}{dt} \text{Tr}(\rho) = \sum_{\mu} \eta_\mu \gamma_\mu (\text{Tr}(\rho) - 1) \langle L_\mu^\dagger L_\mu \rangle$ . If  $\text{Tr}(\rho_0) = 1$ , the NLME is trace-preserving, i.e.  $\text{Tr}(\rho(t)) = 1$ .

Property III: No conservation under strong symmetry. For the LME in Eq. (1), the strong symmetry condition

$$[U, H] = [U, L_\mu] = 0, \text{ for all } \mu, \quad (10)$$

can guarantee the conservation of the observation  $O$ , where  $U = e^{i\theta O}$  is the continuous symmetry with  $\theta \in \mathbb{R}$  [47, 48].

However, for the NLME, the strong symmetry condition leads to

$$\frac{d}{dt}\text{Tr}(O\rho) = \sum_{\mu} \eta_{\mu} \gamma_{\mu} (\text{Tr}(O\rho) - 1) \langle L_{\mu}^{\dagger} L_{\mu} \rangle, \quad (11)$$

where a non-zero  $\eta_{\mu}$  can break the conservation of  $O$ .

Properties I and II unveil that the NLME is Hermiticity-preserving and trace-preserving for a real physics process. Property III indicates that the nonlinearity breaks the conservation law.

According to whether it can be reduced to LME, the NLME can be divided into trivial and nontrivial classes. When  $L_{\mu}^{\dagger} L_{\mu} \rho(t) = \lambda_{\mu} \rho(t)$  holds for all  $\mu$ , the NLME becomes

$$\frac{d\rho}{dt} = -i[H, \rho] + \sum_{\mu=1}^M (1 - \eta_{\mu}) \gamma_{\mu} \left( L_{\mu} \rho L_{\mu}^{\dagger} - \frac{1}{2} \{L_{\mu}^{\dagger} L_{\mu}, \rho\} \right), \quad (12)$$

which is just the LME in Eq. (1) with  $\gamma_{\mu} \rightarrow \gamma_{\mu}^{eff} = (1 - \eta_{\mu}) \gamma_{\mu}$ . We call this case as a trivial class where the postselection can be regarded as a weakening of the coupling from the environment. There is a sufficient condition for the trivial class:

$$L_{\mu}^{\dagger} L_{\mu} \rho_0 = \lambda_{\mu} \rho_0, [L_{\mu}^{\dagger} L_{\mu}, H] = [L_{\mu}^{\dagger} L_{\mu}, L_k] = 0 \text{ for all } \mu, k, \quad (13)$$

where  $\rho_0$  is the initial state. Systems decaying by Pauli operators belong to the trivial class, because  $L_{\mu}^{\dagger} L_{\mu}$  is an identity matrix.

For a translational invariant system, the condition (13) expands to

$$\Gamma \rho_0 = \lambda \rho_0, [\Gamma, H] = [\Gamma, L_k] = 0 \text{ for all } k, \quad (14)$$

where  $\Gamma = \sum_{\mu} L_{\mu}^{\dagger} L_{\mu}$ . An example with continuous measurements of particle numbers is shown in the Supplemental Material [45].

**Postselected skin effect.**— Now we study a model in the nontrivial class, which exhibits skin effect induced by postselection. Considering a  $L$ -site free fermion chain under open boundary condition monitored by  $L + 1$  detectors with unified efficiency  $\eta$  as shown in Fig. 2 (a), the corresponding NLME is given by

$$\begin{aligned} \frac{d\rho}{dt} = & -i[H, \rho] + \\ & \sum_{l=0}^L \gamma_l \left( -\frac{1}{2} \{L_l^{\dagger} L_l, \rho\} + (1 - \eta) L_l \rho L_l^{\dagger} + \eta \langle L_l^{\dagger} L_l \rangle \rho \right), \end{aligned} \quad (15)$$

where  $H = J \sum_{l=1}^{L-1} a_l^{\dagger} a_{l+1} + h.c.$ ,  $\gamma_l = \gamma$ ,  $L_l = d_l^{\dagger} d_l$  with  $d_l = (a_l + i a_{l+1}) / \sqrt{2}$  [29] for  $l = 1 \sim L - 1$ ,  $\gamma_0 = \gamma_L = \gamma/2$ ,  $L_0 = \hat{n}_1$  and  $L_L = \hat{n}_L$ . For simplicity, we set  $\gamma \leq J = 1$ .

When  $\eta = 0$ , the evolution equation reduces to LME. The Hermiticity of  $L_l$  ensures the identity matrix is a steady-state solution of Eq. (15), which means the steady state exhibits a uniform distribution on the lattice, as shown in Fig. 3 (f). However, when  $\eta \neq 0$ , the particles will accumulate on one

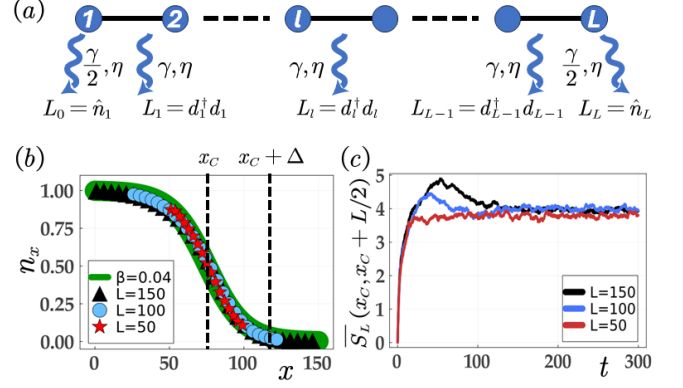


FIG. 2. (a) Illustration of the model with postselected skin effect. (b) Steady-state distributions of the half-filled chain with 50 (red star), 100 (blue circle), and 150 (black triangle) sites. The green line is the fitting function Eq. (16) with  $\beta = 0.04$ . (c) Evolution of half-chain entanglement entropy defined by Eq. (19) in the half-filled chain with 50 (red line), 100 (blue line), and 150 (black line) sites. In (b) and (c),  $\gamma = 0.4$ ,  $\eta = 0.6$  and the initial state is  $|1010\dots\rangle$ . The results are an average of 60 quantum trajectories by the Monte Carlo wavefunction method with time step  $\delta t = 0.005$ .

side, as shown in Fig. 2 (b). The steady-state population in a half-filled chain is well fitted by a tanh function:

$$n(x) = -\frac{1}{2} \tanh\left(\beta\left(x - \frac{L+1}{2}\right)\right) + 0.5, \quad (16)$$

where  $n(x)$  is the particle number on the site  $x$ . The fitting parameter  $\beta$  is determined by  $\gamma$  and  $\eta$ , and it is almost unchanged for different lattice sizes. In Fig. 2 (b), the steady states of different sizes are fitted with the same  $\beta$  (green line). Since the skin steady state is induced by a postselected processes, we call this phenomenon as the postselected skin effect.

To explain the postselected skin effect, we rewrite Eq. (15) as Eq. (7), with

$$H_{eff}(\eta\gamma) = \sum_{l=1}^{L-1} \left( (J - \eta\gamma/4) a_{l+1}^{\dagger} a_l + (J + \eta\gamma/4) a_l^{\dagger} a_{l+1} \right) \quad (17a)$$

$$\mathcal{L}_M(\rho) = \sum_{l=0}^L (1 - \eta) \gamma \left( 1 - \frac{\delta_{l0} + \delta_{lL}}{2} \right) \left( L_l \rho L_l^{\dagger} - \frac{1}{2} \{L_l^{\dagger} L_l, \rho\} \right) \quad (17b)$$

$$\mathcal{L}_N(\rho) = -\frac{1}{2} \eta \gamma \left\langle \sum_{l=1}^{L-1} j_l \right\rangle \rho, \quad (17c)$$

where  $j_l = -i(a_{l+1}^{\dagger} a_l - a_l^{\dagger} a_{l+1})$ . Since the pure measurement term  $\mathcal{L}_M$  and the normalization term  $\mathcal{L}_N$  do not offer a bias force on particles, the non-Hermitian  $H_{eff}$  as a Hatano-Nelson model [49, 50] will drive particles gathering on the left side, as long as  $\eta\gamma \neq 0$ .

The value of  $\beta$  reflects the strength of postselected skin effect. There are two mechanisms to increase  $\beta$ . One is increasing  $\gamma$ , which transfers the dynamics from a non-dissipative

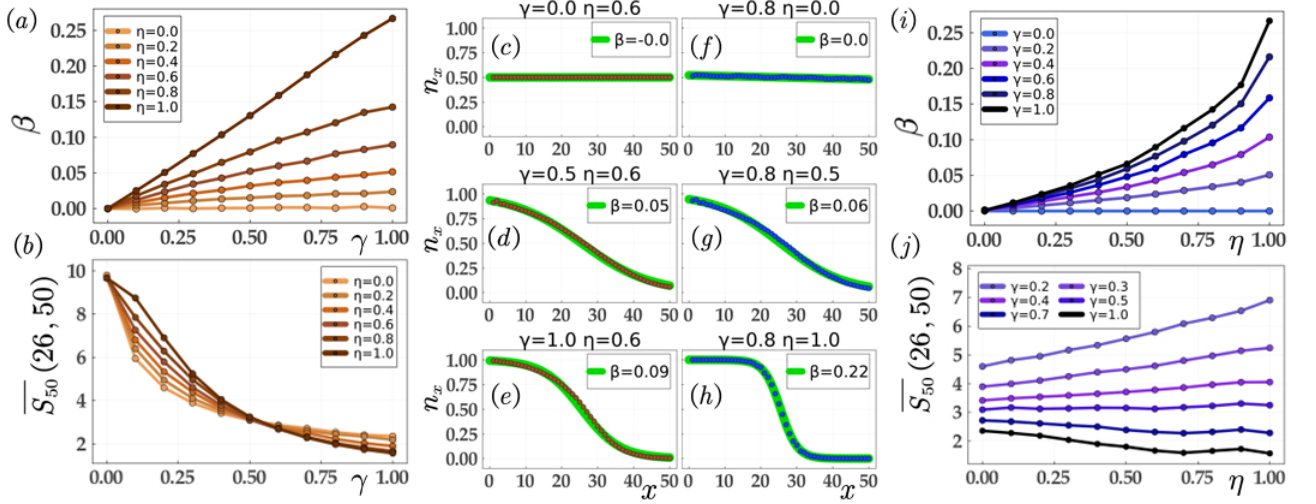


FIG. 3. (a) The fitting parameter  $\beta$  and (b) the half-chain entanglement entropy  $\bar{S}_L(x_C, x_C + L/2)$  of the steady state as a function of  $\gamma$  with different  $\eta$ , where  $\beta$  has linear relationship with  $\gamma$  implying a scale invariance of steady state in terms of  $1/\gamma$ . (c) ~ (h) Steady-state distribution with different  $\gamma$  and  $\eta$  (points from numerical results and green lines from function fitting). (i)  $\beta$  and (j)  $\bar{S}_L(x_C, x_C + L/2)$  of the steady state as a function of  $\eta$  with different  $\gamma$ , where the entropy lines show different monotonicity of  $\eta$  as a result from the combining of Zeno effect and skin effect. In all subfigures, results are from an average of 60 quantum trajectories in a half-filled 50-site chain by Monte Carlo wave-function method with time step  $\delta t = 0.005$ .

free system to NLME. Populations of steady states with different  $\gamma$  are shown in Figs. 3 (c) ~ (e). The other one is increasing  $\eta$ , transferring the dynamics from LME to ENHH, as shown in Figs. 3 (f) ~ (h). While  $\beta$  increases linearly with  $\gamma$ , it increases nonlinearly with  $\eta$ , as shown in Figs. 3 (a) and (i). As for the linear growth, we set  $\beta = k\gamma$ , then the distribution function in Eq. (16) becomes

$$n(x) = -\frac{1}{2} \tanh\left(k \frac{x - (L+1)/2}{1/\gamma}\right) + 0.5, \quad (18)$$

which implies a scale invariance of steady state in terms of  $1/\gamma$ .

*Zeno effect versus skin effect.*— Considering  $\beta$  is positive correlation to both  $\gamma$  and  $\eta$ , the steady-state population distribution can not effectively distinguish the different effects induced by the environmental coupling and postselection. Next we demonstrate that the TAAE  $\bar{S}_L(x_C, x_C + \Delta)$  can serve as a good indicator to reflect the intrinsic differences between the two mechanisms, which is defined as

$$\bar{S}_L(x_C, x_C + \Delta) := \lim_{N \rightarrow +\infty} \frac{1}{N} \sum_{i=1}^N -\text{Tr}(\rho_{[x_C, x_C + \Delta]}^i \ln \rho_{[x_C, x_C + \Delta]}^i), \quad (19)$$

where the entropy is an average of  $N$  trajectories in a  $L$ -site chain, and  $\rho_{[x_C, x_C + \Delta]}^i$  is the reduced density matrix of the pure state in the  $i$ -th trajectory on the subinterval  $[x_C, x_C + \Delta]$ , where  $x_C$  is the middle point of the chain and  $\Delta$  is the interval length, as shown in Fig. 2 (b). The time evolution of half-chain entropy  $\bar{S}_L(x_C, x_C + L/2)$  is shown in Fig. 2 (c).

As shown in Fig. 2 (b) and (j), the steady-state TAAE exhibits different features in terms of  $\gamma$  and  $\eta$ . It monotonically

decreases with increasing  $\gamma$ . However, it shows different monotonicity of  $\eta$  with different  $\gamma$ . The differences come from the combining of Zeno effect [51] from the measurement term  $\mathcal{L}_M$  and skin effect from  $H_{eff}(\eta\gamma)$ . When  $\gamma$  increases, TAAE is suppressed both by the increasing strength of  $\mathcal{L}_M$  and the larger nonreciprocity of  $H_{eff}(\eta\gamma)$ . When  $\eta$  increases, the TAAE is governed by the competition between the decrease in Zeno effect and increase in skin effect. The above processes are expressed as

$$\gamma \uparrow \Rightarrow \begin{cases} \text{Zeno effect} \uparrow \Rightarrow \text{Entropy} \downarrow \\ \text{Skin effect} \uparrow \Rightarrow \text{Entropy} \downarrow \end{cases} \quad (20a)$$

$$\eta \uparrow \Rightarrow \begin{cases} \text{Zeno effect} \downarrow \Rightarrow \text{Entropy} \uparrow \\ \text{Skin effect} \uparrow \Rightarrow \text{Entropy} \downarrow \end{cases} \quad (20b)$$

From Fig. 2 (j), when  $\gamma$  is small, the entropy increases with  $\eta$ , which implies the measurement effects playing a dominant role. When  $\gamma$  is large, the entropy is decreasing with  $\eta$ , implying the dominant role of the non-Hermitian skin effect.

*Distribution and scaling of entangled entropy.*— The post-selected skin effect profoundly affects the distribution and scaling behaviors of TAAE by the tanh-fitting steady state, where the particle number only changes rapidly in the middle of the chain. Near the ends of a long chain, the local site is nearly fully occupied ( $n_x \approx 1$ ) or near vacuum ( $n_x \approx 0$ ), which contributes little to entangled entropy. This makes the entropy distribution  $\bar{S}_L(x_C, x_C + \Delta)$  increase with a small  $\Delta$  while saturate for large  $\Delta$ , as shown in Fig. 4 (a).

The steady state's scaling behavior of the half-chain TAAE  $\bar{S}_L(x_C, x_C + L/2)$  also presents a two-segment structure. When increasing  $L$ , the population distribution of the whole chain

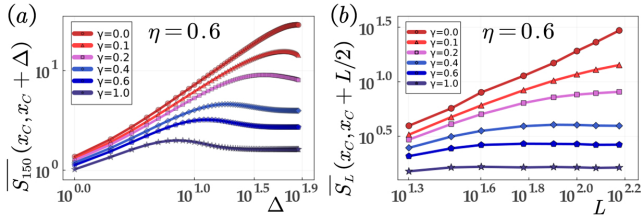


FIG. 4. (a) Steady-state entanglement entropy  $\bar{S}_L(x_C, x_C + \Delta)$  as a function of the bipartition size  $\Delta$  in a half-filled 150-site chain with  $\eta = 0.6$  and  $\gamma$  from 0 to 1 in the log-log plot. (b) Half-chain entanglement entropy  $\bar{S}_L(x_C, x_C + L/2)$  scaling with the half-filled chain length  $L$  in the log-log plot. The entropy has a two-segment scaling behavior: algebraic growth in small  $L$  and saturation in large  $L$ . With decreasing  $\gamma$ , the algebraic growth segment becomes longer. Especially in  $\gamma = 0$ , the growth segment increases to the whole chain, which implies a volume law of entropy in the non-dissipative free systems.

becomes a larger part of the tanh function Eq. (16), as shown in Fig (2) (b), and meanwhile the end-site particle number  $n_L$  decreases rapidly from 0.5 and then approaches slowly to 0. This leads to  $\bar{S}_L(x_C, x_C + L/2)$  having an algebraic growth in small  $L$  and saturation in large  $L$ , as shown in Fig (4) (b).

The above analysis can help us understand the transition from the area law of TAEE with skin effect to the volume law in non-dissipative free systems ( $\gamma = 0$ ). Due to  $\beta = k\gamma$ , decreasing  $\gamma$  will make the tanh function change slower, which brings a bigger algebraic growth interval. When  $\gamma = 0$ , the whole chain is in the growth segment, giving rise to the volume law of entangled entropy.

**Summary.**— We proposed a NLME to describe the postselection dynamics of the open quantum system. By reducing quantum jumps, this equation continuously interpolates between LME and ENHH. While NLME keeps Hermiticity and trace-preserving for physical processes, the nonlinearity can break the conservation law under strong symmetry conditions. According to whether it can be reduced to the LME, we can divide NLME into trivial and nontrivial classes. A model in the nontrivial class is then presented to showcase the postselected skin effect, where the steady state exhibits distribution with particles biased to one side as long as a few quantum jumps are discarded. The steady-state distribution from postselected skin effect is well fitted by a scale-invariant tanh function, which profoundly affects the distribution and scaling behaviors of steady-state TAEE. We also demonstrated that the TAEE can effectively distinguish the different influence from the environment and postselection.

**Acknowledgments.**— We thank Y.-P. Wang for helpful discussions on the Gaussian-state method. This work is supported by National Key Research and Development Program of China (Grant No. 2023YFA1406704 and 2021YFA1402104), the NSFC under Grants No. 12174436 and No. T2121001, and the Strategic Priority Research Program of Chinese Academy of Sciences under Grant No. XDB33000000.

\* [schen@iphy.ac.cn](mailto:schen@iphy.ac.cn)

- [1] G. Lindblad, On the generators of quantum dynamical semigroups, *Commun.Math. Phys.* **48**, 119-130 (1976).
- [2] V. Gorini, A. Kossakowski, and E. C. G. Sudarshan, Completely positive dynamical semigroups of N-level systems, *J. Math. Phys.* **17**, 821 (1976).
- [3] C. W. Gardiner and M. J. Collett, Input and output in damped quantum systems: Quantum stochastic differential equations and the master equation, *Phys. Rev. A* **31**, 3761 (1985).
- [4] D. Manzano, A short introduction to the Lindblad master equation, *AIP Advances* **10**, 025106 (2020).
- [5] X. Niu, J. Li, S. L. Wu, and X. X. Yi, Effect of quantum jumps on non-Hermitian systems, *Phys. Rev. A* **108**, 032214 (2023).
- [6] J. Dalibard, Y. Castin, and K. Mølmer, Wave-function approach to dissipative processes in quantum optics, *Phys. Rev. Lett.* **68**, 580 (1992).
- [7] R. Dum, P. Zoller, and H. Ritsch, Monte Carlo simulation of the atomic master equation for spontaneous emission, *Phys. Rev. A* **45**, 4879 (1992).
- [8] R. Dum, A. S. Parkins, P. Zoller, and C. W. Gardiner, Monte Carlo simulation of master equations in quantum optics for vacuum, thermal, and squeezed reservoirs, *Phys. Rev. A* **46**, 4382 (1992).
- [9] K. Mølmer, C. Yvan, and D. Jean, Monte Carlo wavefunction method in quantum optics, *J. Opt. Soc. Am. B* **10**, 524 (1993).
- [10] M. B. Plenio and P. L. Knight, The quantum-jump approach to dissipative dynamics in quantum optics, *Rev. Mod. Phys.* **70**, 101 (1998).
- [11] A. J. Daley, Quantum trajectories and open many-body quantum systems, *Advances in Physics* **63**, 77 (2014).
- [12] W. Nagourney, J. Sandberg, and H. Dehmelt, Shelved optical electron amplifier: Observation of quantum jumps, *Phys. Rev. Lett.* **56**, 2797 (1986).
- [13] T. Sauter, W. Neuhauser, R. Blatt, and P. E. Toschek, Observation of Quantum Jumps, *Phys. Rev. Lett.* **57**, 1696 (1986).
- [14] J. C. Bergquist, R. G. Hulet, W. M. Itano, and D. J. Wineland, Observation of Quantum Jumps in a Single Atom, *Phys. Rev. Lett.* **57**, 1699 (1986).
- [15] S. Gleyzes, S. Kuhr, C. Guerlin, J. Bernu, S. DelSéglise, U. Busk Hoff, M. Brune, J.-M. Raimond, and S. Haroche, Quantum jumps of light recording the birth and death of a photon in a cavity, *Nature* **446** (2007), 10.1038/nature05589.
- [16] K. W. Murch, S. J. Weber, C. Macklin, and I. Siddiqi, Observing single quantum trajectories of a superconducting quantum bit, *Nature* **502** (2013), 10.1038/nature12539.
- [17] Z. K. Mineev, S. O. Mundhada, S. Shankar, P. Reinhold, R. Gutiérrez-Jáuregui, R. J. Schoelkopf, M. Mirrahimi, H. J. Carmichael, and M. H. Devoret, To catch and reverse a quantum jump mid-flight, *Nature* **570** (2019), 10.1038/s41586-019-1287-z.
- [18] C.W. von Keyserlingk, Tibor Rakovszky, Frank Pollmann, and S. L. Sondhi, Operator Hydrodynamics, OTOCs, and Entanglement Growth in Systems without Conservation Laws, *Phys. Rev. X* **8**, 021013 (2018).
- [19] A. Nahum, S. Vijay and J. Haah, Operator Spreading in Random Unitary Circuits *Phys. Rev. X* **8**, 021014 (2018).
- [20] Y. Li, X. Chen, and M. P. A. Fisher, Quantum zeno effect and the many-body entanglement transition, *Phys. Rev. B* **98**, 205136 (2018).
- [21] B. Skinner, J. Ruhman, and A. Nahum, Measurement-Induced Phase Transitions in the Dynamics of Entanglement, *Phys. Rev.*

- [X 9, 031009 \(2019\)](#).
- [22] Y. Li, X. Chen, and M. P. A. Fisher, Measurement-driven entanglement transition in hybrid quantum circuits, [Phys. Rev. B 100, 134306 \(2019\)](#).
- [23] A. Chan, R. M. Nandkishore, M. Pretko, and G. Smith, Unitary projective entanglement dynamics, [Phys. Rev. B 99, 224307 \(2019\)](#).
- [24] X. Cao, A. Tilloy, and A. D. Luca, Entanglement in a fermion chain under continuous monitoring, [SciPost Phys. 7, 024 \(2019\)](#).
- [25] O. Alberton, M. Buchhold, and S. Diehl, Entanglement Transition in a Monitored Free-Fermion Chain: From Extended Criticality to Area Law, [Phys. Rev. Lett. 126, 170602 \(2021\)](#).
- [26] X. Turkeshi, A. Biella, R. Fazio, M. Dalmonte, and M. Schiró, Measurement-induced entanglement transitions in the quantum Ising chain: From infinite to zero clicks, [Phys. Rev. B 103, 224210 \(2021\)](#).
- [27] M. Coppola, E. Tirrito, D. Karevski, and M. Collura, Growth of entanglement entropy under local projective measurements [Phys. Rev. B 105 094303 \(2022\)](#).
- [28] Y.-N. Zhou, Generalized Lindblad master equation for measurement-induced phase transition [SciPost Phys. Core 6, 023 \(2023\)](#).
- [29] Y.-P. Wang, C. Fang, and J. Ren, Absence of entanglement transition due to feedback-induced skin effect, [arXiv:2209.11241 \[quant-ph\]](#).
- [30] X. Feng, S. Liu, S. Chen, and W. Guo, Absence of logarithmic and algebraic scaling entanglement phases due to the skin effect, [Phys. Rev. B 107, 094309 \(2023\)](#).
- [31] K. Kawabata, T. Numasawa, and S. Ryu, Entanglement Phase Transition Induced by the Non-Hermitian Skin Effect, [Phys. Rev. X 13, 021007 \(2023\)](#).
- [32] K. Li, Z.-C. Liu, and Y. Xu, Disorder-Induced Entanglement Phase Transitions in Non-Hermitian Systems with Skin Effects, [arXiv:2305.12342 \[quant-ph\]](#).
- [33] S.-Z. Li, X.-J. Yu, and Z. Li, Emergent entanglement phase transitions in non-Hermitian Aubry-André-Harper chains, [Phys. Rev. B 109, 024306 \(2024\)](#).
- [34] L. Zhou, Entanglement phase transitions in non-Hermitian quasicrystals, [Phys. Rev. B 109, 024204 \(2024\)](#).
- [35] X. Feng and S. Chen, Boundary-sensitive Lindbladians and relaxation dynamics, [Phys. Rev. B 109, 014313 \(2024\)](#).
- [36] F. Minganti, A. Miranowicz, R. W. Chhajlany, I. I. Arkhipov and F. Nori, Hybrid-Liouvilian formalism connecting exceptional points of non-Hermitian Hamiltonians and Liouvillians via postselection of quantum trajectories, [Phys. Rev. A 101, 062112 \(2020\)](#).
- [37] S. Yao and Z. Wang, Edge States and Topological Invariants of Non-Hermitian Systems, [Phys. Rev. Lett. 121, 086803 \(2018\)](#).
- [38] F. K. Kunst, E. Edvardsson, J. C. Budich, and E. J. Bergholtz, Biorthogonal Bulk-Boundary Correspondence in Non-Hermitian Systems, [Phys. Rev. Lett. 121, 026808 \(2018\)](#).
- [39] C. H. Lee and R. Thomale, Anatomy of skin modes and topology in non-Hermitian systems, [Phys. Rev. B 99, 201103 \(2019\)](#).
- [40] F. Song, S. Yao, and Z. Wang, Non-Hermitian Skin Effect and Chiral Damping in Open Quantum Systems, [Phys. Rev. Lett. 123, 170401 \(2019\)](#).
- [41] C.-H. Liu, K. Zhang, Z. Yang, and S. Chen, Helical damping and dynamical critical skin effect in open quantum systems, [Phys. Rev. Res. 2, 043167 \(2020\)](#).
- [42] P. He, Y.-G. Liu, J.-T. Wang, and S.-L. Zhu, Damping transition in an open generalized Aubry-André-Harper model, [Phys. Rev. A 105, 023311 \(2022\)](#).
- [43] T. Haga, M. Nakagawa, R. Hamazaki, and M. Ueda, Liouvillian Skin Effect: Slowing Down of Relaxation Processes without Gap Closing, [Phys. Rev. Lett. 127, 070402 \(2021\)](#).
- [44] F. Yang, Q.-D. Jiang, and E. J. Bergholtz, Liouvillian skin effect in an exactly solvable model, [Phys. Rev. Res. 4, 023160 \(2022\)](#).
- [45] See Supplemental Material for (i) The derivation of the nonlinear Lindblad master equation, (ii) Vectorization treatment of the model of two-level atom with monitoring its spontaneous emission, (iii) An example in the trivial class: the homogeneous fermion chain under continuous measurements. The supplemental materials include also references [11, 46].
- [46] Y.-G. Liu and S. Chen, Dynamical signatures of the Liouvillian flat band, [Phys. Rev. B 107, 134307 \(2023\)](#).
- [47] B. Buča and T. Prosen, A note on symmetry reductions of the Lindblad equation: transport in constrained open spin chains, [New J. Phys. 14, 073007 \(2012\)](#).
- [48] V. V. Albert and L. Jiang, Symmetries and conserved quantities in Lindblad master equations, [Phys. Rev. A 89, 022118 \(2014\)](#).
- [49] N. Hatano and D. R. Nelson, Localization Transitions in Non-Hermitian Quantum Mechanics, [Phys. Rev. Lett. 77, 570 \(1996\)](#).
- [50] N. Hatano and D. R. Nelson, Vortex Pinning and Non-Hermitian Quantum Mechanics, [Phys. Rev. B 56, 8651 \(1997\)](#).
- [51] B. Misra and E. C. G. Sudarshan, The Zeno's paradox in quantum theory, [J. Math. Phys. 18, 756 \(1977\)](#).

**SUPPLEMENTAL MATERIAL: NONLINEAR LINDBLAD MASTER EQUATION AND POSTSELECTED SKIN EFFECT**

**S1. The derivation of the nonlinear Lindblad master equation**

Quantum trajectory methods interpret the Lindblad master equation (LME) Eq. (1) in the main text as a stochastic average over individual trajectories of pure states [11]. In one trajectory, the system is assumed in  $|\phi(t)\rangle$  at time  $t$ . After  $\delta t$ , the  $L_\mu$  will make the system jump to the state  $NL_\mu|\phi(t)\rangle$  with the probability of  $\delta p_\mu = \gamma_\mu \delta t \langle \phi(t) | L_\mu^\dagger L_\mu | \phi(t) \rangle$  or evolve to the state  $N \exp(-\frac{1}{2} \gamma_\mu L_\mu^\dagger L_\mu \delta t) |\phi(t)\rangle$  with the probability of  $1 - \delta p_\mu$ . The different jump operators can be regarded as independent measurements by the multiplication rule in probability when  $\delta \rightarrow 0$ . So the state at  $t + \delta t$  is

$$|\phi(t + \delta t)\rangle = e^{-iH\delta t} \mathcal{N} \left\{ \begin{array}{l} (1) \left\{ \begin{array}{l} \delta p_1 : L_1 \\ 1 - \delta p_1 : \exp(-\frac{1}{2} \gamma_1 L_1^\dagger L_1 \delta t) \end{array} \right\} \\ \vdots \\ (\mu) \left\{ \begin{array}{l} \delta p_\mu : L_\mu \\ 1 - \delta p_\mu : \exp(-\frac{1}{2} \gamma_\mu L_\mu^\dagger L_\mu \delta t) \end{array} \right\} \\ \vdots \\ (M) \left\{ \begin{array}{l} \delta p_M : L_M \\ 1 - \delta p_M : \exp(-\frac{1}{2} \gamma_M L_M^\dagger L_M \delta t) \end{array} \right\} \end{array} \right\} |\phi(t)\rangle. \quad (S1)$$

Now, we monitor the jump from  $L_\mu$  by a detector with efficiency  $\eta_\mu$  ( $0 \leq \eta_\mu \leq 1$ ) and postselect the trajectories where no jumps are detected. Averaging these trajectories is equivalent to redistributing the probabilities of measurement results by the substitution  $\delta p_\mu \rightarrow (1 - \eta_\mu) \delta p_\mu$ . Then the state at  $t + \delta t$  is

$$|\phi(t + \delta t)\rangle = e^{-iH\delta t} \mathcal{N} \left\{ \begin{array}{l} (1) \left\{ \begin{array}{l} (1 - \eta_1) \delta p_1 : L_1 \\ 1 - (1 - \eta_1) \delta p_1 : \exp(-\frac{1}{2} \gamma_1 L_1^\dagger L_1 \delta t) \end{array} \right\} \\ \vdots \\ (\mu) \left\{ \begin{array}{l} (1 - \eta_\mu) \delta p_\mu : L_\mu \\ 1 - (1 - \eta_\mu) \delta p_\mu : \exp(-\frac{1}{2} \gamma_\mu L_\mu^\dagger L_\mu \delta t) \end{array} \right\} \\ \vdots \\ (M) \left\{ \begin{array}{l} (1 - \eta_M) \delta p_M : L_M \\ 1 - (1 - \eta_M) \delta p_M : \exp(-\frac{1}{2} \gamma_M L_M^\dagger L_M \delta t) \end{array} \right\} \end{array} \right\} |\phi(t)\rangle. \quad (S2)$$

Making the first-order approximation of  $\delta t$ , the maximum probability state  $|\phi_{eff}\rangle$  and its probability  $P_{Max}$  in Eq. (S2) are

$$P_{Max} = \prod_\mu [1 - (1 - \eta_\mu) \delta p_\mu] \approx 1 - \sum_\mu (1 - \eta_\mu) \delta p_\mu, \quad (S3a)$$

$$|\phi_{eff}\rangle = e^{-iH\delta t} \mathcal{N} \left( \prod_\mu \exp(-\frac{1}{2} \gamma_\mu L_\mu^\dagger L_\mu \delta t) \right) |\phi(t)\rangle \approx \mathcal{N} \exp(-iH_{eff} \delta t) |\phi(t)\rangle, \quad (S3b)$$

where  $H_{eff}(\gamma) = H - \frac{i}{2} \sum_\mu \gamma_\mu L_\mu^\dagger L_\mu$ . The second highest probability comes from jumping only once in  $M$  measurements. The state  $|\phi_\mu\rangle$  related to  $L_\mu$  and its probability  $P_\mu$  are

$$P_\mu = (1 - \eta_\mu) \delta p_\mu \prod_{j \neq \mu} [1 - (1 - \eta_j) \delta p_j] \approx (1 - \eta_\mu) \delta p_\mu \quad (S4a)$$

$$|\phi_\mu\rangle = e^{-iH\delta t} \mathcal{N} \left( \prod_{j \neq \mu} \exp(-\frac{1}{2} \gamma_j L_j^\dagger L_j \delta t) \right) L_\mu |\phi(t)\rangle \approx \mathcal{N} \exp(-iH\delta t) L_\mu |\phi(t)\rangle. \quad (S4b)$$

Then the nonlinear Lindblad master equation (NLME) is obtained by

$$\begin{aligned} \frac{d}{dt} \rho &= \lim_{\delta t \rightarrow 0} \frac{1}{\delta t} (|\phi(t + \delta t)\rangle \langle \phi(t + \delta t)| - |\phi(t)\rangle \langle \phi(t)|) \\ &= \lim_{\delta t \rightarrow 0} \frac{1}{\delta t} \left( P_{Max} |\phi_{eff}\rangle \langle \phi_{eff}| + \left( \sum_\mu P_\mu |\phi_\mu\rangle \langle \phi_\mu| \right) - |\phi(t)\rangle \langle \phi(t)| \right) \\ &= -i[H, \rho] + \sum_\mu \gamma_\mu \left( -\frac{1}{2} \{L_\mu^\dagger L_\mu, \rho\} + (1 - \eta_\mu) L_\mu \rho L_\mu^\dagger + \eta_\mu \langle L_\mu^\dagger L_\mu \rangle \rho \right). \end{aligned} \quad (S5)$$

### S2. Vectorization treatment of the two-level atom

The Eq. (9) in the main text describes the postselection dynamics of the two-level atom with monitoring its spontaneous emission. We can deal with it by vectorization method [46]. First the density matrix  $\rho$  is mapped to the density vector  $|\rho\rangle$ :

$$\rho = \begin{pmatrix} \rho_{ee} & \rho_{eg} \\ \rho_{ge} & \rho_{gg} \end{pmatrix} \rightarrow |\rho\rangle = (\rho_{ee}, \rho_{eg}, \rho_{ge}, \rho_{gg})^T. \quad (\text{S6})$$

Second, the NLME is mapped as

$$\frac{d}{dt} |\rho\rangle = L_\eta |\rho\rangle, \quad (\text{S7})$$

where

$$L_\eta = -iH \otimes I + iI \otimes H^\dagger - \frac{\gamma}{2}(L^\dagger L \otimes I + I \otimes L^T L^*) + (1-\eta)\gamma L \otimes L^* + \eta\gamma \langle L^\dagger L \rangle, \quad (\text{S8})$$

where

$$H = \begin{pmatrix} 0 & J \\ J & 0 \end{pmatrix}, \quad L = \begin{pmatrix} 0 & 0 \\ 1 & 0 \end{pmatrix}, \quad I = \begin{pmatrix} 1 & 0 \\ 0 & 1 \end{pmatrix}. \quad (\text{S9})$$

Then we get the vectorized NLME:

$$\frac{d}{dt} \begin{pmatrix} \rho_{ee} \\ \rho_{eg} \\ \rho_{ge} \\ \rho_{gg} \end{pmatrix} = \begin{pmatrix} -iJ(\rho_{ge} - \rho_{eg}) + \eta\gamma\rho_{ee}^2 - \gamma\rho_{ee} \\ -iJ(\rho_{gg} - \rho_{ee}) + \eta\gamma\rho_{eg}\rho_{ee} - 0.5\gamma\rho_{eg} \\ iJ(\rho_{gg} - \rho_{ee}) + \eta\gamma\rho_{ge}\rho_{ee} - 0.5\gamma\rho_{ge} \\ iJ(\rho_{ge} - \rho_{eg}) + \eta\gamma\rho_{gg}\rho_{ee} + (1-\eta)\gamma\rho_{ee} \end{pmatrix} \quad (\text{S10})$$

### S3. An example in the trivial class

Considering a homogeneous fermion chain in periodic boundary condition under continuous measurements of particle number in every site. The postselection dynamics is described by

$$\begin{aligned} \frac{d\rho}{dt} &= -i[H, \rho] + \gamma \sum_l \left( -\frac{1}{2} \{ \hat{n}_l^2, \rho \} + (1-\eta) \hat{n}_l \rho \hat{n}_l + \eta \langle \hat{n}_l^2 \rangle \rho \right) \\ &= -i[H, \rho] + \gamma \left( -\frac{1}{2} \{ \hat{N}, \rho \} + \sum_l \left( (1-\eta) \hat{n}_l \rho \hat{n}_l + \eta \langle \hat{n}_l \rangle \rho \right) \right), \end{aligned} \quad (\text{S11})$$

where  $H = \sum_{mn} \mathcal{H}_{mn} a_m^\dagger a_n$  is the system Hamiltonian,  $\gamma$  is the measurement strength,  $\eta$  is the efficiency of detectors,  $\hat{n}_l = a_l^\dagger a_l$  is the particle-number operator in the site  $l$ , and  $\hat{N} = \sum_l \hat{n}_l$  is the total particle number operator.

The correlation Matrix  $G$  is defined by  $G_{ij} := \langle a_i^\dagger a_j \rangle = \text{Tr}(a_i^\dagger a_j \rho)$ . By Eq. (S11), we have

$$\frac{d}{dt} G_{ij} = -i(\mathcal{H}^T G - G \mathcal{H}^T)_{ij} - (1-\eta)\gamma(1-\delta_{ij})G_{ij} + \eta\gamma(\langle \hat{N} \rangle G_{ij} - \langle a_i^\dagger a_j \hat{N} \rangle), \quad (\text{S12})$$

and

$$\frac{d}{dt} \langle \hat{N} \rangle = \frac{d}{dt} \sum_l G_{ll} = \eta\gamma(\langle \hat{N} \rangle^2 - \langle \hat{N}^2 \rangle), \quad (\text{S13})$$

When  $\eta\gamma \neq 0$ , the conservation of total particle number requires the fluctuation  $\langle \hat{N} \rangle^2 - \langle \hat{N}^2 \rangle$  is 0, namely  $\rho$  is the eigenmatrix of  $\hat{N}$ .

We have  $[\hat{N}, H] = [\hat{N}, \hat{n}_l] = 0$  and when the initial state is the eigenstate of  $\hat{N}$ , the trivial condition Eq. (14) in the main text is met. Then the Eq. (S11) is reduced to

$$\frac{d\rho}{dt} = -i[H, \rho] + (1-\eta)\gamma \left( -\frac{1}{2} \{ \hat{N}, \rho \} + \sum_l (\hat{n}_l \rho \hat{n}_l) \right). \quad (\text{S14})$$

The above equation is just the LME with the substitution  $\gamma \rightarrow (1-\eta)\gamma$ . It illustrates that, in the trivial class, increasing postselected strength  $\eta$  in NLME is completely equivalent to decreasing the measurement strength  $\gamma$  in LME.